

Dynamics of an air bubble rising in viscosity-stratified fluids

A Thesis Submitted to
Indian Institute of Technology Hyderabad
In Partial Fulfillment of the Requirements for
The Degree of

MASTER OF TECHNOLOGY

by

Premlata Amarnath Ram

Reg. No. CH13M1009



भारतीय प्रौद्योगिकी संस्थान हैदराबाद
Indian Institute of Technology Hyderabad

DEPARTMENT OF CHEMICAL ENGINEERING
INDIAN INSTITUTE OF TECHNOLOGY HYDERABAD
SANGAREDDY, HYDERABAD – 502 285
DECEMBER 2017

DECLARATION

I hereby declare that this written submission represents my ideas in my own words, and where ideas or words of others have been included, I have adequately cited and referenced the original sources. I also declare that I have adhered to all principles of academic honesty and integrity and have not misrepresented or fabricated or falsified any idea/data/fact/source in my submission. I understand that any violation of the above will be a cause for disciplinary action by the Institute and can also evoke penal action from the sources that have thus not been properly cited, or from whom proper permission has not been taken when needed.



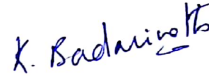
Premalata Amarnath Ram
Roll No: CH13M1009

APPROVAL SHEET

This thesis entitled "Dynamics of an air bubble rising in viscosity-stratified fluids" by Ms. Premlata Amarnath Ram is approved for the degree of Master of Technology from Indian Institute of Technology Hyderabad.



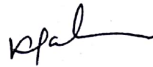
(Dr. Raja Banerjee) External Examiner
Department of Mechanical Engineering
IIT Hyderabad



(Dr. Karri Badarinath) Chairman
Department of Mechanical Engineering
IIT Hyderabad



(Dr. Narasimha Mangadoddy) Internal Examiner
Department of Chemical Engineering
IIT Hyderabad



(Prof. Kirti Chandra Sahu) Adviser
Department of Chemical Engineering
IIT Hyderabad

Acknowledgements

Firstly, I would like to express my sincere gratitude to my advisor Prof. Kirti Chandra Sahu for his continuous support for my M.Tech study. His guidance helped me a lot in all the time of research and writing of this thesis.

I am grateful to my Parents and Siblings, who have provided me moral and emotional support in my life. I am also grateful to my other family members and friends who have supported me along the way.

I thank my fellow lab-mates for their help and support.

Special Thanks to Manoj Kumar Tripathi, for helping me in my research work. I am thankful to our Director and IIT Hyderabad for providing me infrastructure and lab facility. Finally I am thankful to MHRD for the financial support throughout my M.Tech.

Abstract

The bubble rise dynamics in an unconfined quiescent viscosity-stratified medium has been numerically investigated. This is frequently encountered in industrial as well as natural phenomena. In spite of the large number of studies carried out on bubbles and drops, very few studies have examined the influence of viscosity stratification on bubble rise dynamics. To the best of our knowledge, none of them have isolated the effects of viscosity-stratification alone, even though it is known to influence the dynamics extensively, which is the main objective of the present study. Our results demonstrate some counter-intuitive phenomena for certain range of parameters due to the presence of viscosity stratification in the surrounding fluid. It is also observed that the effect of viscosity stratification is qualitatively different for different regimes of the dimensionless parameters. In future, it will be interesting to investigate this problem in three-dimensions

List of Figures

2.1	Figure represents the schematic of axisymmetric computational domain and center line representing axis of symmetry with cylindrical coordinate. Here Fluid “B” represents the bubble rising inside a viscosity stratified medium (Fluid “A”) under the action of gravity. H and L represents the height and length of computational domain respectively.	3
2.2	The time evolution of the shapes of the bubble for $Ga = 10$, $Eo = 0.2$, $\rho_r = 10^3$, $\mu_r = 10^2$. From left to right and from bottom to top: $t = 0; 0.2; 0.4; 0.6; 0.8; 1; 1.2; 1.4; 1.6; 1.8; 2.2; 2.4; 2.6; 2.8$ and 3 . The shapes of the bubble agree well with those presented in Sussman & Smereka (Sussman & Smereka, 1997).	6
2.3	Comparison of the terminal shapes of the bubble obtained from the present simulations (shown by red lines) with those presented in Bhaga & Weber (Bhaga & Weber, 1981) (background picture) for different values of Ga : (a) $Ga = 0.167$, (b) $Ga = 0.222$, (c) $Ga = 0.355$ and (d) $Ga = 0.586$. The rest of the parameter values are $Eo = 0.021$, $\rho_r = 1.39 \times 10^3$, and $\mu_{r0} = 10^2$.	7
2.4	Comparison of streamline patterns along with the terminal shapes of the bubble (shown by red lines) obtained from the present simulation (on the left hand side of each panel) with those presented in Bhaga & Weber (Bhaga & Weber, 1981) (right hand side of each panel) for (a) $Ga = 0.79$, $Eo = 0.017$, (b) $Ga = 0.9$, $Eo = 0.021$, (c) $Ga = 1.26$, $Eo = 0.017$, (d) $Ga = 1.78$, $Eo = 0.027$, (e) $Ga = 2.19$, $Eo = 0.017$, and (f) $Ga = 3.32$, $Eo = 0.011$. The rest of the parameter values are $\rho_r = 1.39 \times 10^3$ and $\mu_{r0} = 10^2$.	7
3.1	The terminal shapes of the bubble obtained from the present simulation in $Ga - Eo$ space for the constant viscosity case ($a_1 = 1, a_2 = 0$). The rest of the parameter values are $\rho_r = 10^3, \mu_r = 10^2$.	10
3.2	Time evolution of the shapes of the bubble obtained for $Ga = 7.071$ and $Bo = 0.05$ for the constant viscosity case ($a_1 = 1, a_2 = 0$). The rest of the parameter values are $\rho_r = 10^3, \mu_r = 10^2$. The dimensionless time is written at the bottom of each bubbles.	10
3.3	Time evolution of bubble shapes for $Eo = 0.04$: (a) constant viscosity ($a_1 = 1, a_2 = 0$) for $Ga = 2.236$, (b) linearly increasing viscosity ($a_1 = 0.2, a_2 = 0.2$) for $Ga = 2.236$, (c) constant viscosity but with Ga modified based on the maximum viscosity, $Ga_m = 2.236/\mu_A$ (at $z = 30.71$) (d) constant viscosity but with Ga modified based on the minimum viscosity, $Ga_m = 2.236/\mu_A$ (at $z = 0$).	12

3.4	Comparison of the streamlines at $t = 40$ for (a) constant viscosity ($a_1 = 1, a_2 = 0$) for $Ga = 2.236$, (b) linearly increasing viscosity ($a_1 = 0.2, a_2 = 0.2$) for $Ga = 2.236$, (c) constant viscosity but with Ga modified based on the maximum viscosity, $Ga_m = 2.236/\mu_A$ (at $z = 28.9$) (d) constant viscosity but with Ga modified based on the minimum viscosity, $Ga_m = 2.236/\mu_A$ (at $z = 0$). The rest of the parameter values the same as those used to generate Fig. 3.3.	13
3.5	Variation of center of gravity and aspect ratio of the bubble with time. The rest of the parameter values are the same as those used to generate Fig. 3.3.	13
3.6	Comparison between the bubble shape at different time for $EO = 0.02$ and $Ga = 0.2236$ in viscosity stratified medium (a) constant viscosity medium (b) linearly increasing viscosity medium (c) constant viscosity but with Ga modified based on the maximum viscosity, $Ga_m = 0.2236/\mu_A$ (at $z = 13.01$) (d) constant viscosity but with Ga modified based on the minimum viscosity, $Ga_m = 0.2236/\mu_A$ (at $z = 0$).	14
3.7	Comparison of the streamlines at $t = 40$ for $EO = 0.02$ and $Ga = 0.2236$ in viscosity stratified medium (a) constant viscosity medium (b) linearly increasing viscosity medium (c) constant viscosity but with Ga modified based on the maximum viscosity, $Ga_m = 0.2236/\mu_A$ (at $z = 13.01$) (d) constant viscosity but with Ga modified based on the minimum viscosity, $Ga_m = 0.2236/\mu_A$ (at $z = 0$).	15
3.8	Variation of center of gravity and aspect ratio of the bubble with time. The rest of the parameter values are the same as those used to generate Fig. 3.6.	15
3.9	Comparison between the bubble shape at different time for $EO = 0.05$ and $Ga = 0.2236$ in viscosity stratified medium (a) constant viscosity medium (b) linearly increasing viscosity medium (c) constant viscosity but with Ga modified based on the maximum viscosity, $Ga_m = 0.2236/\mu_A$ (at $z = 13.04$) (d) constant viscosity but with Ga modified based on the minimum viscosity, $Ga_m = 0.2236/\mu_A$ (at $z = 0$).	16
3.10	Comparison of the streamlines of bubbles at $t = 40$ for $EO = 0.05$ and $Ga = 0.2236$ in viscosity stratified medium (a) constant viscosity medium (b) linearly increasing viscosity medium (c) constant viscosity but with Ga modified based on the maximum viscosity, $Ga_m = 0.2236/\mu_A$ (at $z = 13.04$) (d) constant viscosity but with Ga modified based on the minimum viscosity, $Ga_m = 0.2236/\mu_A$ (at $z = 0$).	17
3.11	Variation of center of gravity and aspect ratio of the bubble with time. The rest of the parameter values are the same as those used to generate Fig. 3.9.	17
3.12	Comparison between the bubble shape at different time for $EO = 5 \times 10^{-3}$ and $Ga = 0.2236$ in viscosity stratified medium (a) constant viscosity medium (b) linearly increasing viscosity medium (c) constant viscosity but with Ga modified based on the maximum viscosity, $Ga_m = 0.2236/\mu_A$ (at $z = 9.16$) (d) constant viscosity but with Ga modified based on the minimum viscosity, $Ga_m = 0.2236/\mu_A$ (at $z = 0$).	18

3.13	Comparison of the streamlines of bubbles at $t = 25$ for $Eo = 5 \times 10^{-3}$ and $Ga = 0.2236$ in viscosity stratified medium (a) Constant viscosity medium (b) Linearly increasing viscosity medium (c) constant viscosity but with Ga modified based on the maximum viscosity, $Ga_m = 0.2236/\mu_A$ (at $z = 9.16$) (d) constant viscosity but with Ga modified based on the minimum viscosity, $Ga_m = 0.2236/\mu_A$ (at $z = 0$).	19
3.14	Variation of center of gravity and aspect ratio of the bubble with time. The rest of the parameter values are the same as those used to generate Fig. 3.12.	19
3.15	Comparison between the bubble shape at different time for $Eo = 0.05$ and $Ga = 0.707$ in viscosity stratified medium (a) constant viscosity medium (b) linearly increasing viscosity medium (c) constant viscosity but with Ga modified based on the maximum viscosity, $Ga_m = 0.707/\mu_A$ (at $z = 22.06$) (d) constant viscosity but with Ga modified based on the minimum viscosity, $Ga_m = 0.2236/\mu_A$ (at $z = 0$).	20
3.16	Comparison of the streamlines of bubbles at $t = 40$ for $Eo = 5 \times 10^{-3}$ and $Ga = 0.2236$ in viscosity stratified medium (a) Constant viscosity medium (b) Linearly increasing viscosity medium (c) constant viscosity but with Ga modified based on the maximum viscosity, $Ga_m = 0.707/\mu_A$ (at $z = 22.06$) (d) constant viscosity but with Ga modified based on the minimum viscosity, $Ga_m = 0.707/\mu_A$ (at $z = 0$).	21
3.17	Variation of center of gravity and aspect ratio of the bubble with time. The rest of the parameter values are the same as those used to generate Fig. 3.15.	21

List of Tables

Contents

Acknowledgements	iii
Abstract	v
List of Figures	ix
List of Tables	xi
1 Introduction	1
2 Formulation and numerical methods	3
2.1 Formulation	4
2.2 Numerical methods and Validation	5
2.3 Validations	5
2.3.1 Comparison with numerical results of Sussman & Smereka (1997)	5
2.3.2 Comparison with experimental results of Bhaga & Weber (1981)	6
3 Result and Discussion	9
3.1 Linearly increasing viscosity, $\mu_A = \mu_{r0}(a_1 + a_2z)$	9
3.1.1 Point A: $Ga = 2.24, Eo = 0.04$	9
3.1.2 Point B: $Ga = 0.2236, Eo = 0.02$	14
3.1.3 Point C: $Ga = 0.2236, Eo = 0.05$	16
3.1.4 Point D: $Ga = 0.2236, Eo = 5 \times 10^{-3}$	18
3.1.5 Point E: $Ga = 0.707, Eo = 0.05$	20

4 Conclusions	23
----------------------	-----------

Bibliography	25
---------------------	-----------

CHAPTER 1

Introduction

Bubbles rising in a quiescent liquid have been of interest for more than a century, due to its relevance in many natural phenomena, such as aerosol transfer from sea, oxygen dissolution in lakes due to rain and electrification of atmosphere by sea bubbles (Blanchard, 1962), carbon sequestration (Gal-Or *et al.*, 1969), and in industrial applications, such as bubble column reactors. The dynamics of single bubbles have been studied in great detail by Davies & Taylor (1950). Also, rising bubbles in systems with temperature gradients (Tripathi *et al.*, 2015a) have been studied and the effect of marangoni forces on the rise velocity and the arrest conditions have been reported. To our knowledge, no work has been done on the effect of viscosity stratification on the single rising bubble dynamics. Viscosity gradients appear often in systems having temperature gradients or changes in concentration of some solute like sugar, salt etc. Naturally, viscosity varies drastically inside the oceans within a few kilometres distance. Study of rising bubble in such systems may be interesting to industries related to carbon sequestration or bubble column reactors, and to academicians for the scientific curiosity.

The viscosity stratification can occur due to several factors, due to the presence of temperature or concentration gradients in some species/solutes. For instance, the viscosity of water or milk is made to increase by almost three orders of magnitude by the addition of only 2% carboxymethylcellulose (CMC) (Ghannam & Esmail, 1997) in the ice-cream and lotion industries. Note that the density changes due to such an addition of the species (CMC) are negligible while varying the viscosity by a large amount. The viscosity in the underground crude oil reservoirs may vary upto three orders of magnitude (Beal *et al.*, 1946). Also, viscosity of molten silicates and metals can be made to vary across several orders of magnitude (Urbain *et al.*, 1982) by maintaining a temperature difference of a few hundreds of degrees Celsius between the top and the bottom wall of a domain. However, the gradients of temperature or concentration at the liquid-gas interface can also give rise to surface tension gradients, which in turn induce tangential stresses, known as Marangoni stresses (Balasubramaniam, 1998; Balasubramaniam & Subramaniam, 1996; Balasubramaniam & Subramaniam, 2000; Subramanian, 1981, 1983; Subramanian *et al.*, 2002; Tripathi *et al.*, 2015b; Young *et al.*, 1959).

The bubble dynamics due to temperature gradient was first studied by Young *et al.* (1959). They experimentally investigated rise of small or large air bubbles in a container heated from below. For smaller air bubbles, they found that for some imposed temperature gradient, the induced Marangoni stresses acting in the downward direction overcome the buoyancy force, and the bubbles move in the downward direction. However, larger bubbles continue to move in the upward direction. In the later case buoyancy force overcomes the thermocapillary force. Since then this problem has been studied experimentally, numerically and theoretically by several researchers (Subramanian, 1981, 1983; Subramanian *et al.*, 2002; Young *et al.*, 1959).

By conducting numerical simulation, Merritt *et al.* (1993) studied that effect of buoyancy and thermocapillarity on rising bubble dynamics. In the limit of large Reynolds and Marangoni number, Balasubramaniam 1998 studied this problem by an asymptotic analysis. Later Zhang *et al.* (2001) found that inclusion of inertia is crucial in the development of an asymptotic solution for small Marangoni num-

bers in the presence of temperature field. These studies, although took the viscosity stratification due to temperature gradient into account, the influence of viscosity stratification alone was not provided.

Viscosity stratifications achieved due to the presence of temperature and concentration gradients are continuous. Gradual viscosity variation can be naturally found in the mantle liquid below earth's crust and ocean. The stratification can also be achieved without the presence of temperature and concentration gradients. In several applications(Govindarajan & Sahu, 2014), immiscible fluid-layers of almost the same density, but significant viscosity jump are observed. Bubble rise through an interface of two immiscible liquids of different viscosities have been studied in the past by several researchers(Bonhomme *et al.*, 2012; Kemiha *et al.*, 1991; Manga & Stone, 1995). Practically, all phenomena concerning viscosity stratification invariably include density gradient and other factors, which also influence the dynamics. Although, viscosity stratification is expected to play a significant role, with all the factor included, it is impossible to isolate the effect of viscosity stratification from the dynamics of rising bubble.

CHAPTER 2

Formulation and numerical methods

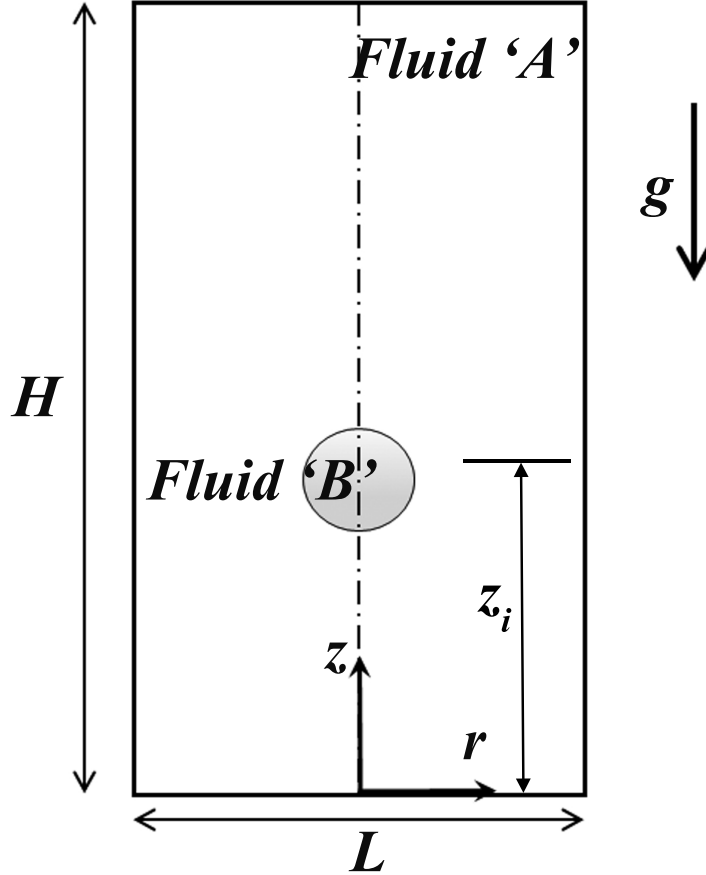


Figure 2.1: Figure represents the schematic of axisymmetric computational domain and center line representing axis of symmetry with cylindrical coordinate. Here Fluid "B" represents the bubble rising inside a viscosity stratified medium (Fluid "A") under the action of gravity. H and L represents the height and length of computational domain respectively.

In this chapter we have described the numerical methods and their validations. The dynamics of an axisymmetric air bubble (designated by fluid 'A') of initial radius R , having constant viscosity μ_B rising under the action of buoyancy inside unbounded domain consisting of another fluid (designated by fluid 'A'), as shown in Fig. 2.1 is numerically investigated using volume-of-fluid (VoF) approach. Both the fluids are considered to be incompressible and Newtonian. The viscosity and density of fluids A and B are μ_A, ρ_A and μ_B, ρ_B , respectively. We use cylindrical coordinates (r, z) to model the rising bubble dynamics starting from a position $z_i = 4R$ in quiescent liquid at time, $t = 0$. Here, r and z are the radial and vertical coordinates, respectively. The viscosity field of fluid 'A', μ_A is initialized as $\mu_A = \mu_0(a_1 + a_2z)$, μ_0 being the viscosity of fluid 'A' at $z = z_i$, and a_1, a_2 are constants, which are defined below. The flow dynamics

is assumed to be symmetrical about $r = 0$, and the acceleration due to gravity, g is acting in the negative z direction, as shown in Fig. 2.1.

2.1 Formulation

The governing equations describing the flow characteristics are:

$$\nabla \cdot \mathbf{u} = 0, \quad (2.1)$$

$$\rho \left[\frac{\partial \mathbf{u}}{\partial t} + \mathbf{u} \cdot \nabla \mathbf{u} \right] = -\nabla p + \nabla \cdot [\mu(\nabla \mathbf{u} + \nabla \mathbf{u}^T)] + \delta \sigma \kappa \mathbf{n} - \rho g \vec{e}_z, \quad (2.2)$$

$$\frac{\partial c}{\partial t} + \mathbf{u} \cdot \nabla c = 0, \quad (2.3)$$

$$\frac{\partial \mu}{\partial t} + \mathbf{u} \cdot \nabla \mu = 0, \quad (2.4)$$

Here, $\mathbf{u}(u, v)$ and p denote the velocity and pressure fields, respectively, wherein u and v are the velocity components in the radial and vertical directions, respectively; c is the volume fraction of the fluid A, which takes on values between 0 and 1 for the air and liquid phases, respectively; μ is the viscosity field which is advected with the local velocity of the fluid; δ is the Dirac delta function; $\kappa = \nabla \cdot \mathbf{n}$ is the curvature in which \mathbf{n} is the unit normal to the interface pointing towards fluid A, \vec{e}_z represents the unit vector in the vertical direction, and σ is the interfacial tension coefficient of the liquid gas interface.

The density, ρ is calculated as a volume averaged quantity as follows:

$$\rho = \rho_B(1 - c) + \rho_A c. \quad (2.5)$$

The following scaling is employed in order to render the governing equations dimensionless:

$$(r, z) = R(\tilde{r}, \tilde{z}), \quad t = \frac{R}{V} \tilde{t}, \quad (u, v) = V(\tilde{u}, \tilde{v}), \quad p = \rho_B V^2 \tilde{p}, \quad \mu = \tilde{\mu} \mu_0, \quad \rho = \tilde{\rho} \rho_B, \quad (2.6)$$

where R is the initial radius of the bubble, the velocity scale is $V = \sqrt{gR}$, and the tildes designate dimensionless quantities. After dropping tildes from all non-dimensional terms, the governing dimensionless equations are given by:

$$\nabla \cdot \mathbf{u} = 0, \quad (2.7)$$

$$\rho \left[\frac{\partial \mathbf{u}}{\partial t} + \mathbf{u} \cdot \nabla \mathbf{u} \right] = -\nabla p + \frac{1}{Ga} \nabla \cdot [\mu(\nabla \mathbf{u} + \nabla \mathbf{u}^T)] + \frac{\delta}{Bo} \hat{\mathbf{n}} \nabla \cdot \hat{\mathbf{n}} - \rho \vec{e}_z, \quad (2.8)$$

$$\frac{\partial c}{\partial t} + \mathbf{u} \cdot \nabla c = 0, \quad (2.9)$$

$$\frac{\partial \mu}{\partial t} + \mathbf{u} \cdot \nabla \mu = 0, \quad (2.10)$$

where $Ga(\equiv \rho_B VR/\mu_B)$ and $Eo(\equiv \rho_B g R^2/\sigma)$ denote the Galileo number and Eötvös number, respectively. The dimensionless density ρ is given by:

$$\rho = (1 - c) + \rho_r c, \quad (2.11)$$

and the initial viscosity field is given by:

$$\mu = (1 - c) + \mu_{r0}(a_1 + a_2 z)c \quad (2.12)$$

where $\mu_{r0} \equiv \mu_0/\mu_B$ and $\rho_r \equiv \rho_B/\rho_A$. Note that setting $a_1 = 1$ and $a_2 = 0$ gives a system with constant viscosity of the surrounding fluid.

2.2 Numerical methods and Validation

In this present study, a finite-volume open source code, *Gerris* (Popinet, 2003; Tripathi *et al.*, 2014) is used to solve the dimensionless governing equations (2.7)-(2.9). The interface between the two fluids is tracked using the volume-of-fluid (VOF) approach with dynamic adaptive grid refinement based on the vorticity magnitude and the position of the interface. *Gerris* uses a generalized height-function method for calculating the curvature of the interface, thus improving the accuracy of the surface tension force calculation for the VOF methods. It is to be noted that *Gerris* minimizes the spurious currents (to the machine error) at the interface (which are known to appear when the density ratio and the interfacial tension are high) by incorporating a balanced force height-function continuum-surface-force formulation (Brackbill *et al.*, 1992; Popinet, 2009) for the inclusion of the surface force term in the Navier-Stokes equations. The flow is assumed to be symmetric about the axis $r = 0$, and the Neumann boundary conditions are imposed at the rest of the boundaries of the computational domain.

2.3 Validations

The *Gerris* solver has been validated extensively by comparing the results obtained from the present simulations with the previously reported numerical and experimental results. We present below a few validation cases relevant to the bubble and drop dynamics

2.3.1 Comparison with numerical results of Sussman & Smereka (1997)

The evolution of shapes of the bubble at different times for $Ga = 10$, $Eo = 0.2$, $\rho_r = 10^3$, $\mu_r = 10^2$ are presented in Fig. 2.2. It can be seen that for this set of parameters the bubble is almost spherical till $t = 0.4$. For $t > 0.4$ the bubble undergoes significant deformation and subsequent topological change at $t = 1.6$. Thereafter the bubble continues to move in the upward direction as an annular doughnut-like structure. It is to be noted here that the bubble shapes presented in Fig. 2.2 are in excellent agreement with the numerical simulation (level-set method) results of Sussman & Smereka (1997) for this set of parameters.

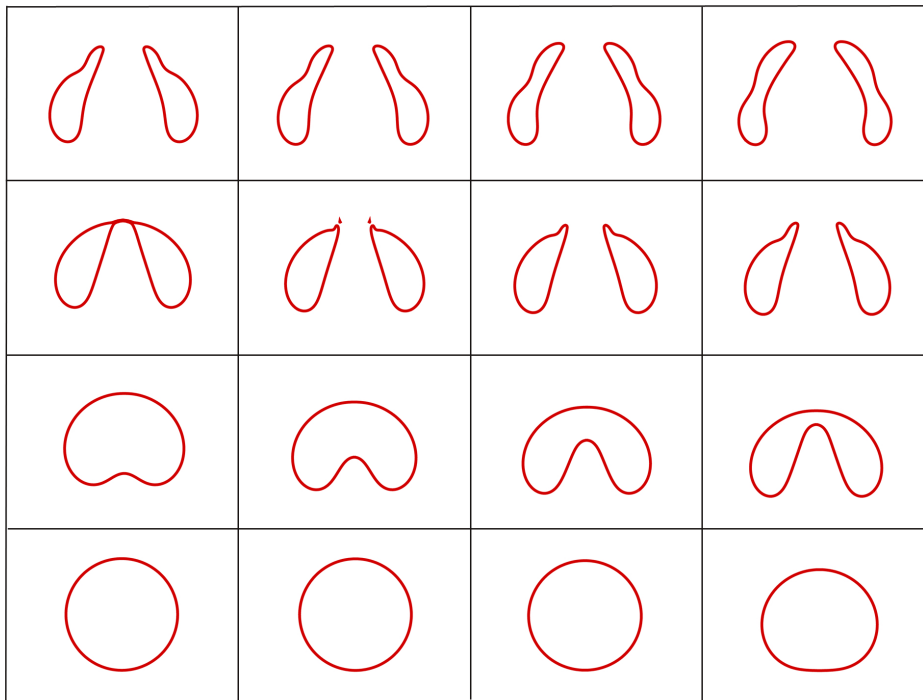


Figure 2.2: The time evolution of the shapes of the bubble for $Ga = 10$, $Eo = 0.2$, $\rho_r = 10^3$, $\mu_r = 10^2$. From left to right and from bottom to top: $t = 0; 0.2; 0.4; 0.6; 0.8; 1; 1.2; 1.4; 1.6; 1.8; 2.2; 2.4; 2.6; 2.8$ and 3 . The shapes of the bubble agree well with those presented in Sussman & Smereka (Sussman & Smereka, 1997).

2.3.2 Comparison with experimental results of Bhaga & Weber (1981)

The terminal shapes and streamlines obtained from our numerical simulation are compared with the experimental results of Bhaga & Weber (Bhaga & Weber, 1981) for different values of Ga and Eo in Figs. 2.3 and 2.4, respectively. In Fig. 2.3, the pictures in the black and white background are the experimental results of Bhaga & Weber (1981) and the red lines show the terminal shape of the bubble obtained from the present simulations. In Fig. 2.4, the left and right hand sides in each panel represent the present simulation results and the experimental results, respectively. It can be seen that the bubble shapes and the streamline patterns are in excellent agreement.

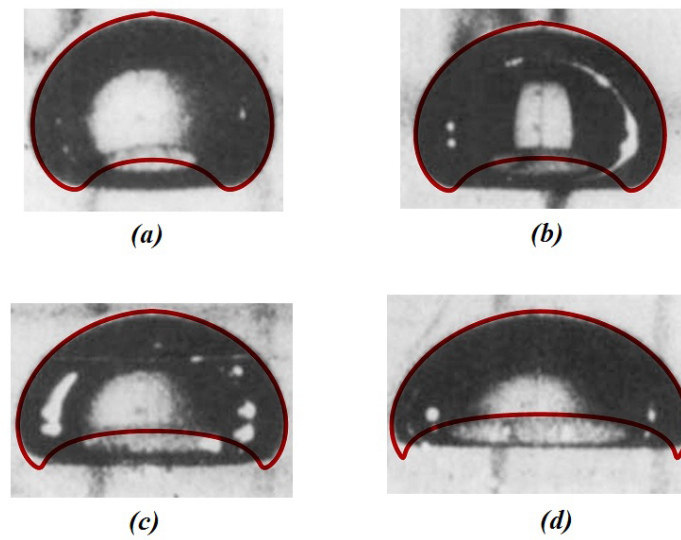


Figure 2.3: Comparison of the terminal shapes of the bubble obtained from the present simulations (shown by red lines) with those presented in Bhaga & Weber (Bhaga & Weber, 1981) (background picture) for different values of Ga : (a) $Ga = 0.167$, (b) $Ga = 0.222$, (c) $Ga = 0.355$ and (d) $Ga = 0.586$. The rest of the parameter values are $Eo = 0.021$, $\rho_r = 1.39 \times 10^3$, and $\mu_{r0} = 10^2$.

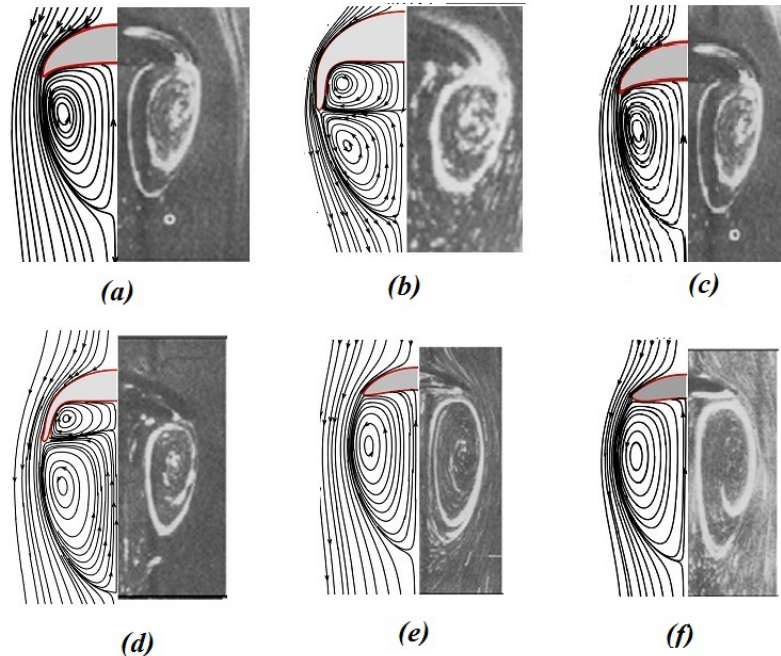


Figure 2.4: Comparison of streamline patterns along with the terminal shapes of the bubble (shown by red lines) obtained from the present simulation (on the left hand side of each panel) with those presented in Bhaga & Weber (Bhaga & Weber, 1981) (right hand side of each panel) for (a) $Ga = 0.79$, $Eo = 0.017$, (b) $Ga = 0.9$, $Eo = 0.021$, (c) $Ga = 1.26$, $Eo = 0.017$, (d) $Ga = 1.78$, $Eo = 0.027$, (e) $Ga = 2.19$, $Eo = 0.017$, and (f) $Ga = 3.32$, $Eo = 0.011$. The rest of the parameter values are $\rho_r = 1.39 \times 10^3$ and $\mu_{r0} = 10^2$.

CHAPTER 3

Result and Discussion

We begin the presentation of our results in Fig. 3.1 by plotting the terminal shapes of the bubble for the constant viscosity case ($a_1 = 1, a_2 = 0$) obtained from our time-dependent simulations in $Ga - Eo$ space. A similar plot based on the steady state calculations was presented by Tsamopoulos *et al.* (2008). Note that in their study, the viscosity and density of the surrounding fluid were used as the characteristic scales to nondimensionalize the governing equations hence a suitable conversion was applied to get our dimensionless variables. We found that for low Ga and low Eo the shapes of the bubble presented in Fig. 3.1 are qualitatively similar to those obtained by Tsamopoulos *et al.* (2008). However, the shapes of the bubble are different for larger values of Eo and Ga . This discrepancy can be attributed to the steady state assumption considered in their study. We also found that the bubble undergoes topological changes and the bubble dynamics remains unsteady for few sets of Ga and Eo (designated by “break-up” in Fig. 3.1). The time evolution of shapes of the bubble for one typical case ($Ga = 7.071$ and $Eo = 0.05$) is shown in Fig. 3.2. It can be seen in this figure that bubble has a different topology for $t > 2$ for this set of parameters. Note that Tsamopoulos *et al.* (2008) also did not find a steady state solution for these parameter values.

The effect of viscosity stratification of the surrounding fluid (for a system where the viscosity increases with increasing z) on the bubble dynamics is investigated next. The viscosity of the surrounding fluid at rest, $t = 0$ is given by:

$$\mu_A = \mu_{r0}(a_1 + a_2 z), \quad (3.1)$$

where values of the constants a_1 and a_2 are fixed at 0.2.

Five typical sets of (Ga, Eo) designated by points A, B, C, D and E in Fig. 3.1 are considered, which correspond to $(Ga, Eo) = (2.24, 0.04), (0.22, 0.02), (0.22, 0.05), (0.22, 0.005),$ and $(0.707, 0.05)$, respectively are investigated below. The behaviour of the rest of the bubbles in Fig. 3.1 can be extrapolated from these typical cases.

3.1 Linearly increasing viscosity, $\mu_A = \mu_{r0}(a_1 + a_2 z)$

3.1.1 Point A: $Ga = 2.24, Eo = 0.04$

The time evolution of shapes of the bubble in linearly increasing viscosity medium (shown in Fig. 3.3(b)) are compared with those of constant viscosity case (shown in Fig. 3.3(a)) for $Ga = 2.236$ and $Eo = 0.04$. It can be seen that for the case of the linearly increasing viscosity medium an elongated skirt (longer than that appears for the constant viscosity case (Fig. 3.3a)) is formed leading to a bigger single recirculation region shown in Fig. 3.4 (b). This is counter intuitive due to the fact that as the bubble rises in the vertical direction the viscosity increases, which in turn decreases the local Ga . It has been observed that at lower Ga the bubble tends to take a dimpled ellipsoidal shape instead of forming a skirt

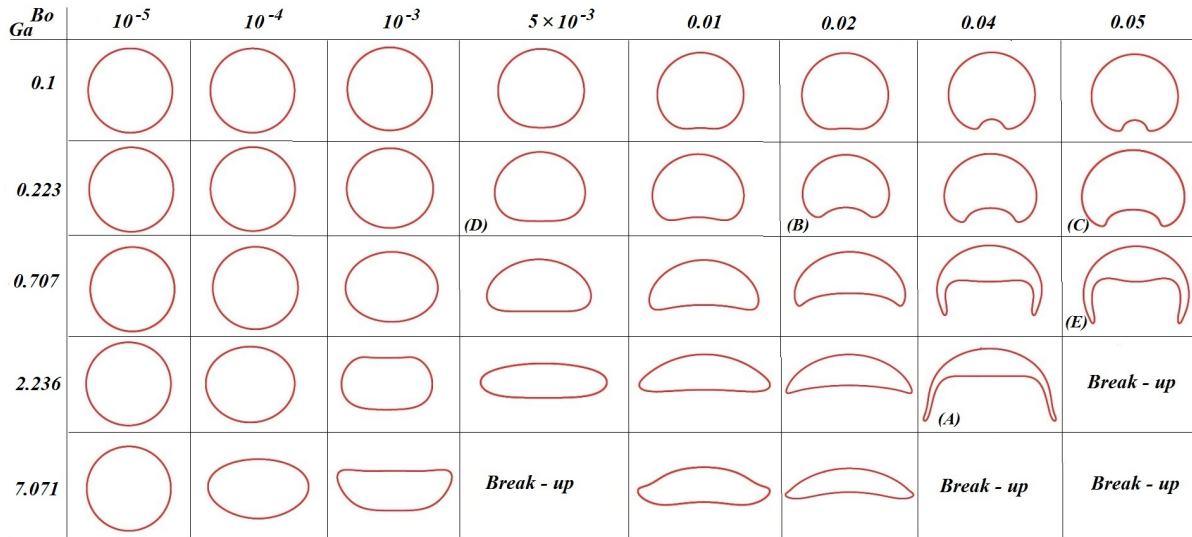


Figure 3.1: The terminal shapes of the bubble obtained from the present simulation in $Ga - Eo$ space for the constant viscosity case ($a_1 = 1, a_2 = 0$). The rest of the parameter values are $\rho_r = 10^3, \mu_r = 10^2$.

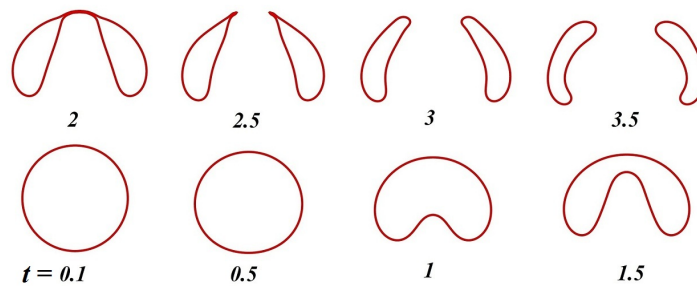


Figure 3.2: Time evolution of the shapes of the bubble obtained for $Ga = 7.071$ and $Bo = 0.05$ for the constant viscosity case ($a_1 = 1, a_2 = 0$). The rest of the parameter values are $\rho_r = 10^3, \mu_r = 10^2$. The dimensionless time is written at the bottom of each bubbles.

(see, for instance the bubble shapes for $EO = 0.04$ in Fig. 3.1). The recirculation zone in the wake of the bubble carries the lower viscosity fluid with it. As a result of this, the contrast in viscosity inside and outside the region surrounded by the skirt continues to increase with the ascent of the bubble. The stresses generated due to the differential viscosity on both sides of the skirt forces it to curl inwards. This interesting deformation of the skirt leads to a physical separation of the two regions with high viscosity contrast by means of the air film contained in the skirt of the bubble. This separation of fluids allows the fast recirculation to occur in the fluid captured inside the wake of the bubble while simultaneously allowing a slow flow outside of the skirt, thus creating a contrast in Reynolds number as well. This may be beneficial to certain processes where a low viscosity fluid is required to be carried through a high viscosity fluid with the help of a carrier bubble.

In order to investigate whether this dynamics is due to our viscosity scale, we re-examine how the results reflect our choice of viscosity scale. In Fig. 3.3(c) and (d) the shapes of the bubble are plotted for constant viscosity case for the same EO , but for Ga modified based on the maximum viscosity of the surrounding fluid at a location upto which the bubble travelled (i.e μ_A at $z = 28.9$), and minimum viscosity (i.e μ_A at $z = 0$) for the linearly increasing case.

As there is no ideal viscosity scale we have made these simplest choices possible. It can be seen in Fig. 3.3 (c) and (d) that the bubble shapes are very different from those observed in Fig. 3.3(b). As expected when the Ga is defined based on the minimum viscosity the bubble quickly undergoes topological changes forming a toroidal shape (doughnut-like structure) for $t > 1.61$. Close inspection of this figure also reveals that the rise velocity of the bubble decreases in the linearly increasing case and also for constant viscosity with Ga defined based on the maximum viscosity as compared that shown in Fig. 3.3(a). Rise velocity is lower than $7a$ for all other cases. It is also observed that when Ga is redefined based on the minimum viscosity the rise velocity decreases (shown in Fig. 3.3(d)) as the bubble undergoes topological changes.

The streamlines plots in Fig. 3.4(a)-(d) correspond to Fig. 3.3(a)-(d), respectively. It can be seen in Fig. 3.4(a) that for constant viscosity case ($Ga = 2.236$) two recirculating regions appear in the wake of the bubble. In case of linearly increasing viscosity case due to the elongated skirt which closes towards the axis of symmetry, a single and bigger recirculation zone is observed in Fig. 3.4(b). However, in Fig. 3.4(c) & (d), which is for constant viscosity but with Ga modified based on the maximum and minimum viscosity respectively, no recirculation zone is found outside the bubble for these parameter values.

The Fig. 3.5(a,b), shows the temporal variation of centre of gravity z_{CG} and aspect ratio a_r of rising bubble respectively, for all the four cases as shown in the Fig. 3.3. Fig. 3.5(a) shows an expected behaviour; the bubbles for constant viscosity cases attend a terminal velocity. However, the bubble in linearly increasing viscosity medium (shown in Fig. 3.3(b)) keeps decelerating, with a peak at an early time (approximately at $t = 2$). The peak may be attributed to the initial acceleration due to buoyancy and the gradual decay in the rise velocity is due to the viscous forces overcoming the gravitational forces at later times. In Fig. 3.5(b), it can be seen that the bubble reaches to a terminal oblate shape for constant viscosity cases. In case of linearly increasing case the bubble becomes oblate by decreasing the a_r to approximately 0.2, but then the aspect ratio increases gradually as the time progress.

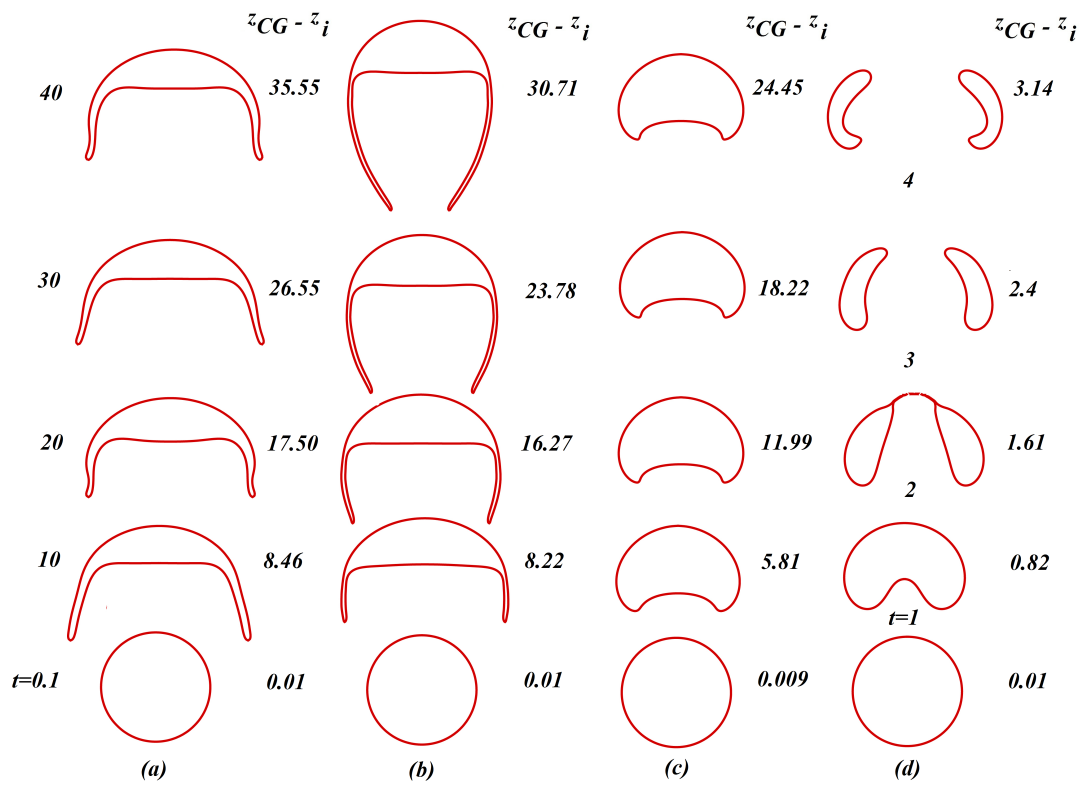


Figure 3.3: Time evolution of bubble shapes for $Eo = 0.04$: (a) constant viscosity ($a_1 = 1, a_2 = 0$) for $Ga = 2.236$, (b) linearly increasing viscosity ($a_1 = 0.2, a_2 = 0.2$) for $Ga = 2.236$, (c) constant viscosity but with Ga modified based on the maximum viscosity, $Ga_m = 2.236/\mu_A$ (at $z = 30.71$) (d) constant viscosity but with Ga modified based on the minimum viscosity, $Ga_m = 2.236/\mu_A$ (at $z = 0$).

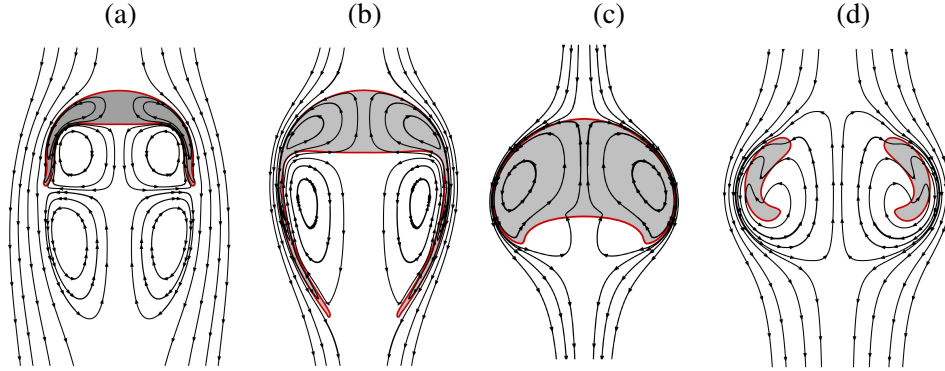


Figure 3.4: Comparison of the streamlines at $t = 40$ for (a) constant viscosity ($a_1 = 1, a_2 = 0$) for $Ga = 2.236$, (b) linearly increasing viscosity ($a_1 = 0.2, a_2 = 0.2$) for $Ga = 2.236$, (c) constant viscosity but with Ga modified based on the maximum viscosity, $Ga_m = 2.236/\mu_A$ (at $z = 28.9$) (d) constant viscosity but with Ga modified based on the minimum viscosity, $Ga_m = 2.236/\mu_A$ (at $z = 0$). The rest of the parameter values the same as those used to generate Fig. 3.3.

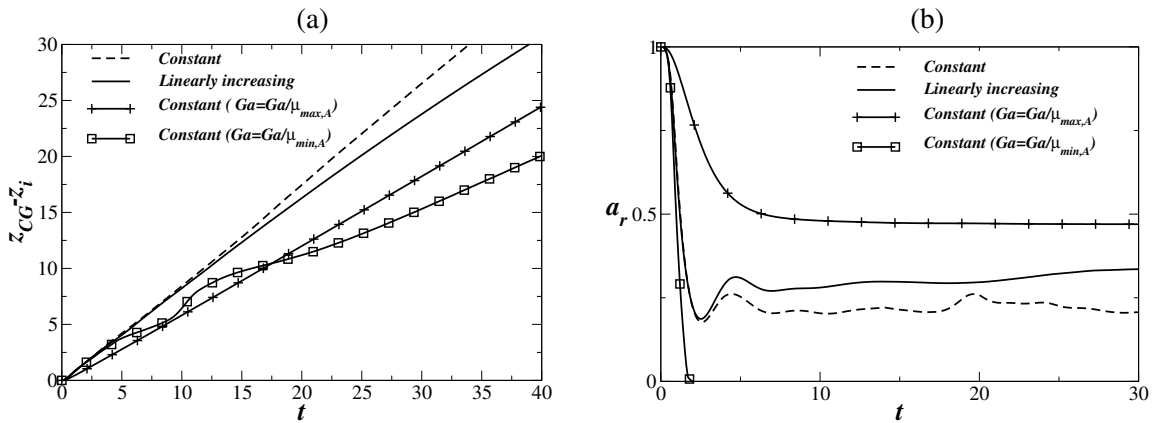


Figure 3.5: Variation of center of gravity and aspect ratio of the bubble with time. The rest of the parameter values are the same as those used to generate Fig. 3.3.

3.1.2 Point B: $Ga = 0.2236, Eo = 0.02$

Next in Fig. 3.6, we investigate the dynamics associated with the bubble marked as point ‘B’ in Fig. 3.1 ($Ga = 0.2236, Eo = 0.02$). In this case, Eo halved and Ga decreases ten times than that of the value used for the bubble designated by point ‘A’. It can be seen in Fig. 3.6 that the shapes of the bubble at different times for linearly increasing viscosity medium (panel b) and constant viscosity system ($a_1 = 1, a_2 = 0$) (panel a) are similar. However, these are qualitatively different from the shapes exhibited by bubble in Fig. 3.6 (c) and (d). This result also suggests that the bubble dynamics is predominantly dominated by governed by the wake region of the bubble. Inspection of this figure also reveals that the dimpled shape of the bubbles in panels (a) and (b) are elliptical, but in panel (c) the shape of the bubble is more or less spherical and in panel (d) the shape of the bubble looks like inverted moon, that is deformation is more here as Ga is modified based on the minimum viscosity $Ga_m = 0.2236/\mu_A$.

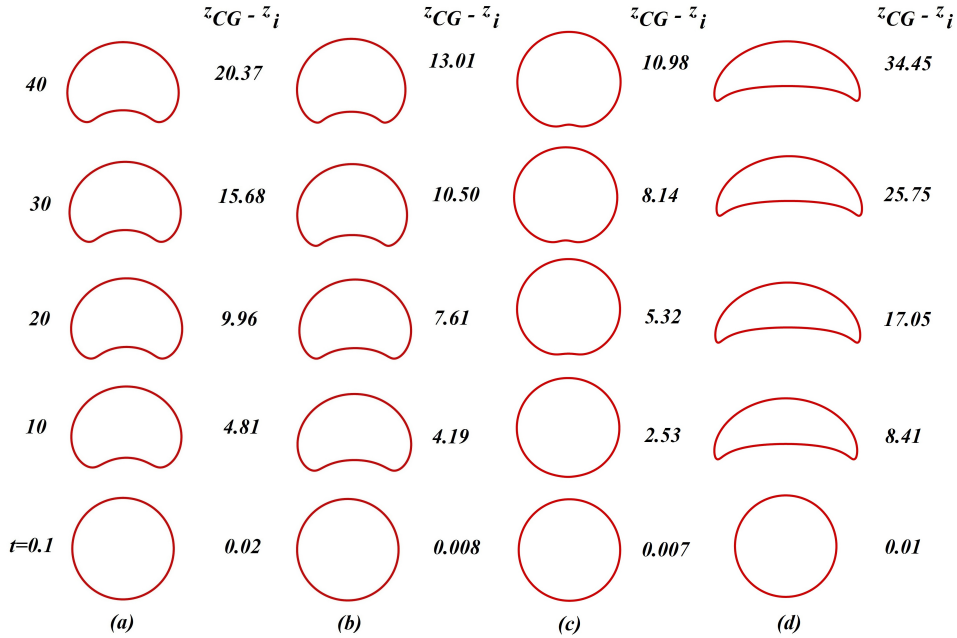


Figure 3.6: Comparison between the bubble shape at different time for $Eo = 0.02$ and $Ga = 0.2236$ in viscosity stratified medium (a) constant viscosity medium (b) linearly increasing viscosity medium (c) constant viscosity but with Ga modified based on the maximum viscosity, $Ga_m = 0.2236/\mu_A$ (at $z = 13.01$) (d) constant viscosity but with Ga modified based on the minimum viscosity, $Ga_m = 0.2236/\mu_A$ (at $z = 0$).

The streamlines plots in Fig. 3.7(a)-(d) correspond to Fig. 3.6(a)-(d), respectively. It can be seen in Fig. 3.7 (a), (b) and (c) that the two recirculating region appears inside the bubble and which suggest that bubble has reached to a terminal shape. In case of Fig. 3.7 (d) since the Ga is modified based on the minimum viscosity $Ga_m = 0.2236/\mu_A$, the deformation is more here and the bubble has not reach to terminal shape, as the streamlines crosses the air-liquid interface, which implies that the shape is far from steady state.

The variation of center of gravity and aspect ratio of the bubble with time generated using the parameter values the same as those used in Fig. 3.6 are shown in Fig. 3.8(a) and (b), respectively. It can be seen in Fig. 3.8(a), for constant viscosity case the bubble is moving fast compare to linearly increasing viscosity medium, which is expected, as in linearly increasing viscosity case, the local viscosity is in-

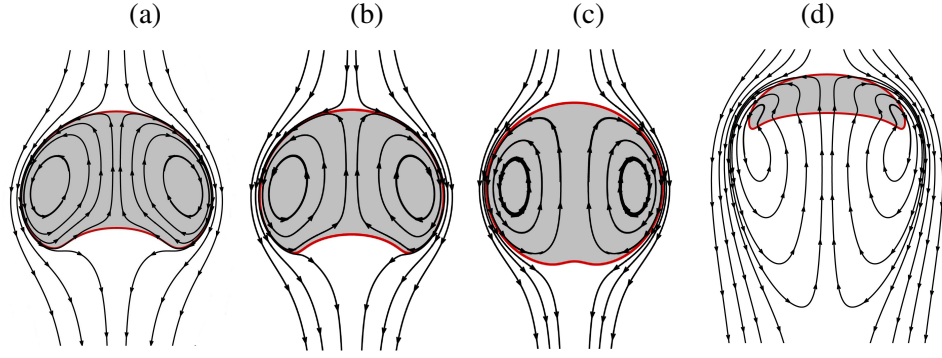


Figure 3.7: Comparison of the streamlines at $t = 40$ for $Eo = 0.02$ and $Ga = 0.2236$ in viscosity stratified medium (a) constant viscosity medium (b) linearly increasing viscosity medium (c) constant viscosity but with Ga modified based on the maximum viscosity, $Ga_m = 0.2236/\mu_A$ (at $z = 13.01$) (d) constant viscosity but with Ga modified based on the minimum viscosity, $Ga_m = 0.2236/\mu_A$ (at $z = 0$).

creasing and hence the velocity of the bubble is decreasing. For constant viscosity but with Ga modified based on the maximum viscosity, $Ga_m = 0.2236/\mu_A$ (at $z = 13.01$) case, the bubble is moving slow compare to all other cases, which is due to the reason as the resultant Ga value will be less compare to base Ga and hence the bubble will move slowly. For constant viscosity but with Ga modified based on the minimum viscosity, $Ga_m = 0.2236/\mu_A$ (at $z = 0$), the bubble is moving very fast compare to all other cases because as the modified Ga is high compare to all other cases and hence the velocity is highest. In Fig. 3.8(b) shows that the aspect ratio of the bubble. For linearly increasing viscosity medium, the forms an oblate shape, after which the bubble has a tendency to go towards the original shape. Whereas for constant viscosity case, the bubble has reached to a terminal oblate shape. For constant viscosity but with Ga modified based on the minimum viscosity, $Ga_m = 0.2236/\mu_A$ (at $z = 0$), the shape of the bubble is more or less spherical and for constant viscosity but with Ga modified based on the maximum viscosity, $Ga_m = 0.2236/\mu_A$ (at $z = 13.01$) case, the bubble is deformation is the most.

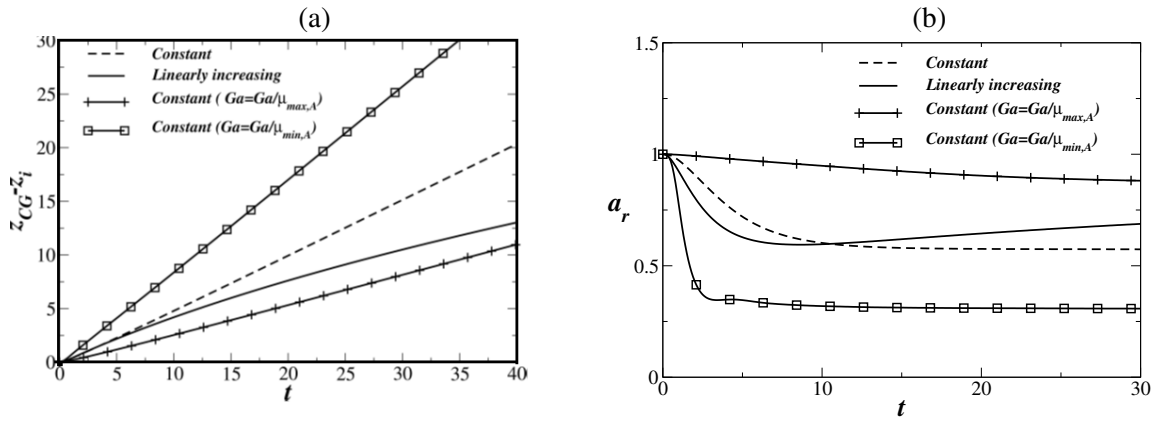


Figure 3.8: Variation of center of gravity and aspect ratio of the bubble with time. The rest of the parameter values are the same as those used to generate Fig. 3.6.

3.1.3 Point C: $Ga = 0.2236, Eo = 0.05$

Next in Fig. 3.9, we investigate the dynamics associated with the bubble marked as point ‘C’ in Fig. 3.1 ($Ga = 0.223, Eo = 0.05$). In this case, Eo increases slightly and Ga decreases ten times than that of the value used for the bubble designated by point ‘A’. Here also, it can be seen in Fig. 3.9 that the shapes of the bubble at different times for linearly increasing viscosity medium (panel b) and constant viscosity system ($a_1 = 1, a_2 = 0$) (panel a) are similar. However, these are qualitatively different from the shapes exhibited by bubble in Fig. 3.9 (c) and (d). Inspection of these figure also reveals that the dimpled shape of the bubbles in panels (a) and (b) are elliptical, but in panel (c) the shape of the bubble is more or less spherical and in panel (d) skirt has formed in the peripheral region.

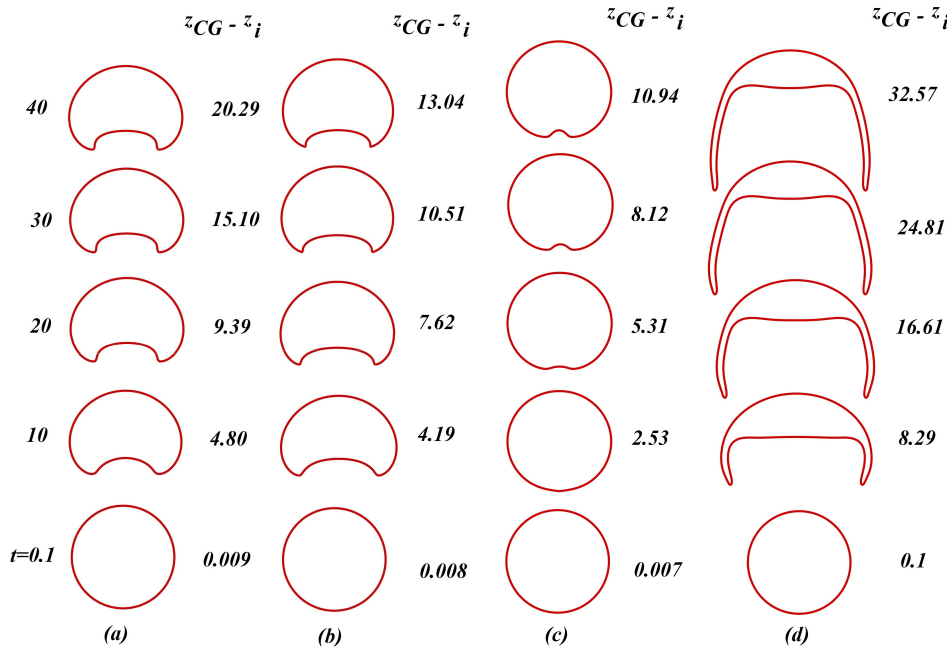


Figure 3.9: Comparison between the bubble shape at different time for $Eo = 0.05$ and $Ga = 0.22361$ in viscosity stratified medium (a) constant viscosity medium (b) linearly increasing viscosity medium (c) constant viscosity but with Ga modified based on the maximum viscosity, $Ga_m = 0.2236/\mu_A$ (at $z = 13.04$) (d) constant viscosity but with Ga modified based on the minimum viscosity, $Ga_m = 0.2236/\mu_A$ (at $z = 0$).

The streamlines plots in Fig. 3.10 (a)-(d) correspond to Fig. 3.9 (a)-(d), respectively. It can be seen in Fig. 3.10 (a) and (c) that the two recirculating region appears inside the bubble and which suggest that bubble has reached to a terminal shape. In case of Fig. 3.10 (b), two recirculating zone appears in the wake region. In Fig. 3.10 (d) since the Ga is modified based on the minimum viscosity $Ga_m = 0.2236/\mu_A$ (at $z = 0$), the deformation is more and the hence the four recirculation zone appears in the wake region.

Fig. 3.11(a) and (b), shows the variation of center of gravity and aspect ratio of the bubble with time generated using the parameter values the same as those used in Fig. 3.9 respectively. Same inference can be made from the Fig. 3.11(a), for constant viscosity case the bubble is moving fast compare to linearly increasing viscosity medium. For constant viscosity but with Ga modified based on the maximum viscosity, $Ga_m = 0.2236/\mu_A$ (at $z = 13.01$) case, the bubble is moving slowly compare to all other cases and for constant viscosity but with Ga modified based on the minimum viscosity, $Ga_m = 0.2236/\mu_A$ (at $z = 0$), the bubble is moving very fastest compare to all other cases. In Fig. 3.11(b) shows that the aspect ratio of the bubble. For linearly increasing viscosity medium, the forms an oblate shape, after

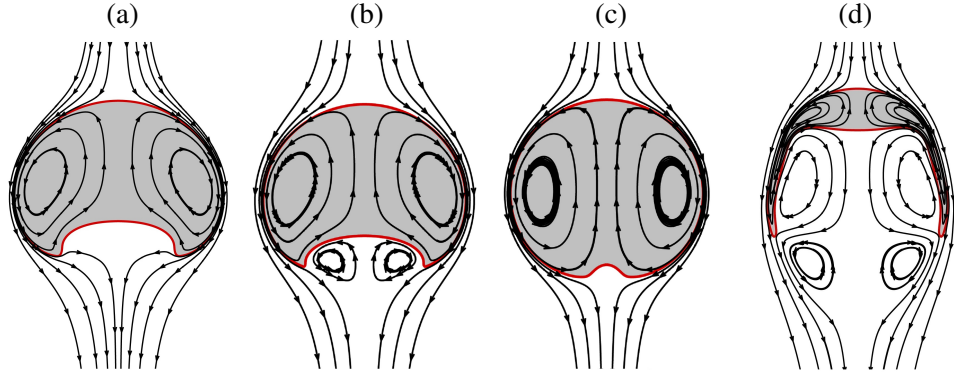


Figure 3.10: Comparison of the streamlines of bubbles at $t = 40$ for $Eo = 0.05$ and $Ga = 0.2236$ in viscosity stratified medium (a) constant viscosity medium (b) linearly increasing viscosity medium (c) constant viscosity but with Ga modified based on the maximum viscosity, $Ga_m = 0.2236/\mu_A$ (at $z = 13.04$) (d) constant viscosity but with Ga modified based on the minimum viscosity, $Ga_m = 0.2236/\mu_A$ (at $z = 0$).

which the bubble has a tendency to go towards the original shape. Whereas for constant viscosity case, the bubble has reached to a terminal oblate shape. For constant viscosity but with Ga modified based on the minimum viscosity, $Ga_m = 0.2236/\mu_A$ (at $z = 0$), the shape of the bubble is more or less spherical and for constant viscosity but with Ga modified based on the maximum viscosity, $Ga_m = 0.2236/\mu_A$ (at $z = 13.04$) case, the bubble is deformation is the most.

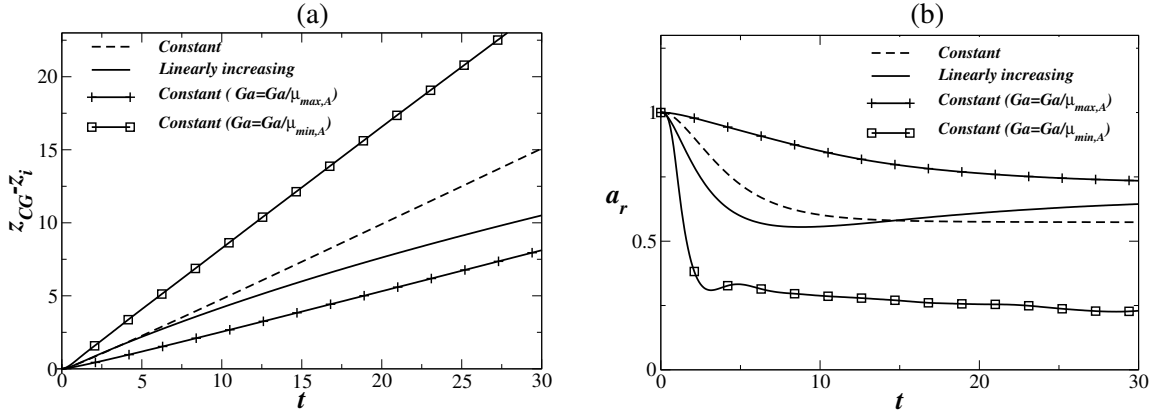


Figure 3.11: Variation of center of gravity and aspect ratio of the bubble with time. The rest of the parameter values are the same as those used to generate Fig. 3.9.

3.1.4 Point D: $Ga = 0.2236, Eo = 5 \times 10^{-3}$

In Fig. 3.12, the shapes of the bubble for $Ga = 0.223, Eo = 5 \times 10^{-3}$ are plotted. Here both Ga and Eo are small. In this case the surface tension dominates the dynamics; the shapes of the bubble become slightly oblate (Fig. 3.12 panel a and b) after reaching an apparent steady state at very early time (for $t > 10$). It can be seen that as the Ga considered in this case is very low, the velocity of the bubbles for constant viscosity cases (panels a) is more as compare to linearly increasing viscosity medium (panel b), because for linearly increasing viscosity case, the velocity of the bubble decreases as the local Ga decreases further due to the increase in local viscosity as the bubble moves in the upward direction. For constant viscosity but with Ga modified based on the maximum viscosity, $Ga_m = 0.2236/\mu_A$ (at $z = 9.16$), bubble deformation is negligible and for constant viscosity but with Ga modified based on the minimum viscosity, $Ga_m = 0.2236/\mu_A$ (at $z = 0$), bubble forms a disk like shape.

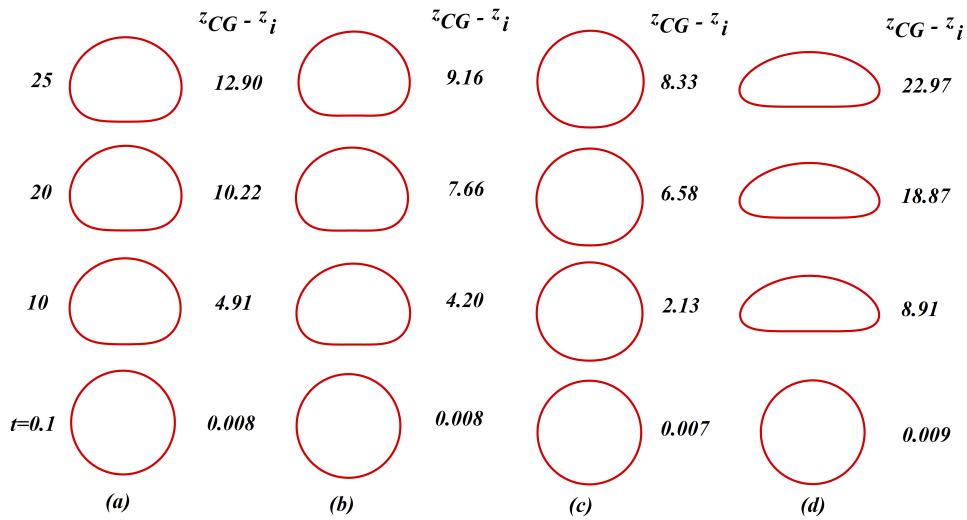


Figure 3.12: Comparison between the bubble shape at different time for $Eo = 5 \times 10^{-3}$ and $Ga = 0.2236$ in viscosity stratified medium (a) constant viscosity medium (b) linearly increasing viscosity medium (c) constant viscosity but with Ga modified based on the maximum viscosity, $Ga_m = 0.2236/\mu_A$ (at $z = 9.16$) (d) constant viscosity but with Ga modified based on the minimum viscosity, $Ga_m = 0.2236/\mu_A$ (at $z = 0$).

The streamlines plots in Fig. 3.13(a)-(d) correspond to Fig. 3.12(a)-(d), respectively. It can be seen in Fig. 3.13 (a), (b) and (c) that the two recirculating region appears inside the bubble and which suggest that bubble has reached to a terminal shape. In case of Fig. 3.13 (d) since the Ga is modified based on the minimum viscosity $Ga_m = 0.2236/\mu_A$ (at $z = 0$), the deformation is more here and two recirculation forms at the wake of the bubble.

Fig. 3.14(a) and (b), shows the variation of center of gravity and aspect ratio of the bubble with time generated using the parameter values the same as those used in Fig. 3.12 respectively. Here also, same inference can be made for the Fig. 3.14(a), as explained in Section 3.1.3, that is, for constant viscosity case the bubble is moving fast compare to linearly increasing viscosity medium. For constant viscosity but with Ga modified based on the maximum viscosity, $Ga_m = 0.2236/\mu_A$ (at $z = 9.16$) case, the bubble is moving slowly compare to all other cases and for constant viscosity but with Ga modified based on the minimum viscosity, $Ga_m = 0.2236/\mu_A$ (at $z = 0$), the bubble is moving very fastest compare to all other cases. In Fig. 3.11(b) shows that the aspect ratio of the bubble. For linearly increasing viscosity medium, the forms an oblate shape, after which the bubble has a tendency to go towards the original

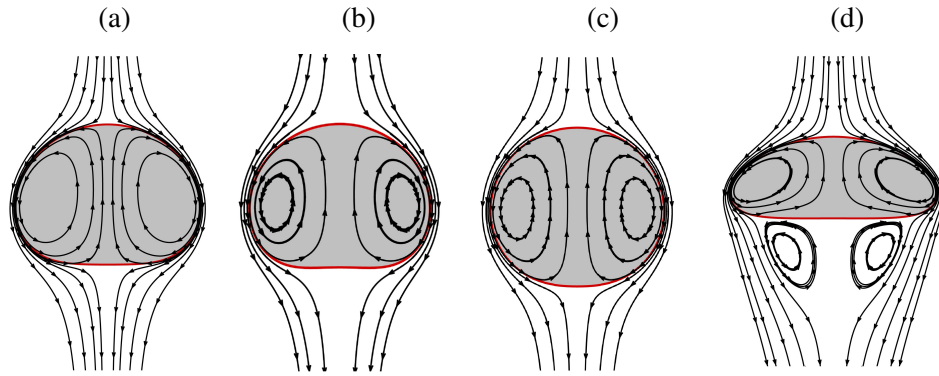


Figure 3.13: Comparison of the streamlines of bubbles at $t = 25$ for $Eo = 5 \times 10^{-3}$ and $Ga = 0.2236$ in viscosity stratified medium (a) Constant viscosity medium (b) Linearly increasing viscosity medium (c) constant viscosity but with Ga modified based on the maximum viscosity, $Ga_m = 0.2236/\mu_A$ (at $z = 9.16$) (d) constant viscosity but with Ga modified based on the minimum viscosity, $Ga_m = 0.2236/\mu_A$ (at $z = 0$).

shape. Whereas for constant viscosity case, the bubble has reached to a terminal oblate shape. For constant viscosity but with Ga modified based on the minimum viscosity, $Ga_m = 0.2236/\mu_A$ (at $z = 0$), the shape of the bubble is more or less spherical and for constant viscosity but with Ga modified based on the maximum viscosity, $Ga_m = 0.2236/\mu_A$ (at $z = 9.16$) case, the bubble is deformation is most .

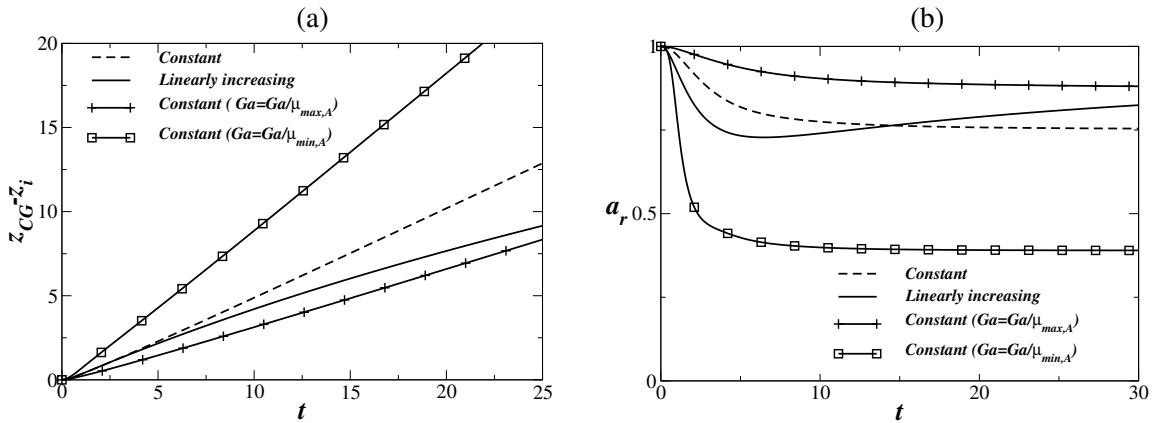


Figure 3.14: Variation of center of gravity and aspect ratio of the bubble with time. The rest of the parameter values are the same as those used to generate Fig. 3.12.

3.1.5 Point E: $Ga = 0.707, Eo = 0.05$

The time evolution of shapes of the bubbles for $Ga = 0.707, Eo = 0.05$ corresponding to the case 'E' in Fig. 3.1 are shown in Fig. 3.15. For panel b, an elongated skirt is formed (compare to panel a) and also a bigger single recirculation region is formed as shown in Fig. 3.16. It can be seen that for panel c, the bubble forms a dimpled shape whereas for panel d the breaks to form satellite bubble. This results demonstrate that, the wake of the bubble plays an important role in skirt formation and also it suggested the there is a significant effect of viscosity stratification on bubble behaviour.

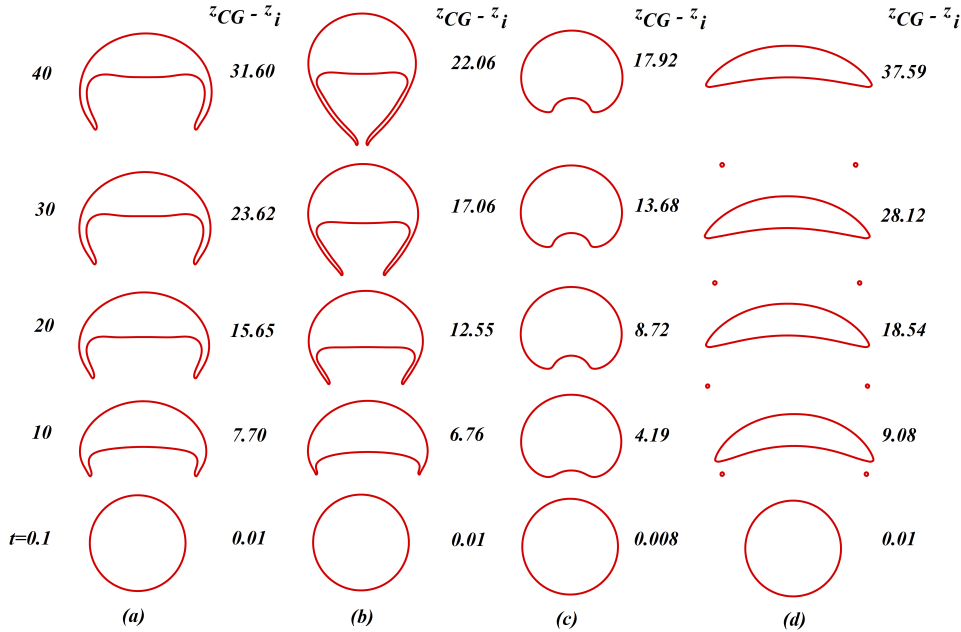


Figure 3.15: Comparison between the bubble shape at different time for $Eo = 0.05$ and $Ga = 0.707$ in viscosity stratified medium (a) constant viscosity medium (b) linearly increasing viscosity medium (c) constant viscosity but with Ga modified based on the maximum viscosity, $Ga_m = 0.707/\mu_A$ (at $z = 22.06$) (d) constant viscosity but with Ga modified based on the minimum viscosity, $Ga_m = 0.2236/\mu_A$ (at $z = 0$).

Fig. 3.17(a) and (b), shows the variation of center of gravity and aspect ratio of the bubble with time generated using the parameter values the same as those used in Fig. 3.12 respectively. Here also, same inference can be made for the Fig. 3.14(a), as explained in Section 3.1.3, that is, for constant viscosity case the bubble is moving fast compare to linearly increasing viscosity medium. For constant viscosity but with Ga modified based on the maximum viscosity, $Ga_m = 0.2236/\mu_A$ (at $z = 9.16$) case, the bubble is moving slowly compare to all other cases and for constant viscosity but with Ga modified based on the minimum viscosity, $Ga_m = 0.2236/\mu_A$ (at $z = 0$), the bubble is moving very fastest compare to all other cases. In Fig. 3.11(b) shows that the aspect ratio of the bubble. For constant viscosity case, the bubble has reached to a terminal oblate shape. For constant viscosity but with Ga modified based on the minimum viscosity, $Ga_m = 0.2236/\mu_A$ (at $z = 0$), the bubble forms a dimpled ellipsoidal shape and for constant viscosity but with Ga modified based on the maximum viscosity, $Ga_m = 0.2236/\mu_A$ (at $z = 9.16$) case, the bubble is deformation is most as it breaks to form satellite bubble.

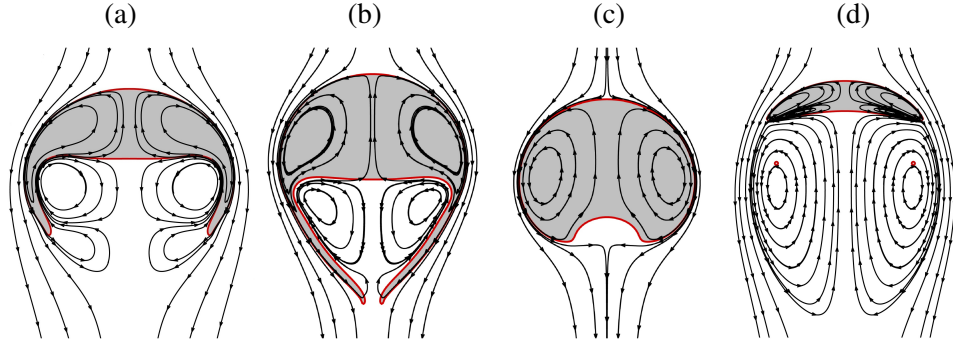


Figure 3.16: Comparison of the streamlines of bubbles at $t = 40$ for $Eo = 5 \times 10^{-3}$ and $Ga = 0.2236$ in viscosity stratified medium (a) Constant viscosity medium (b) Linearly increasing viscosity medium (c) constant viscosity but with Ga modified based on the maximum viscosity, $Ga_m = 0.707/\mu_A$ (at $z = 22.06$) (d) constant viscosity but with Ga modified based on the minimum viscosity, $Ga_m = 0.707/\mu_A$ (at $z = 0$).

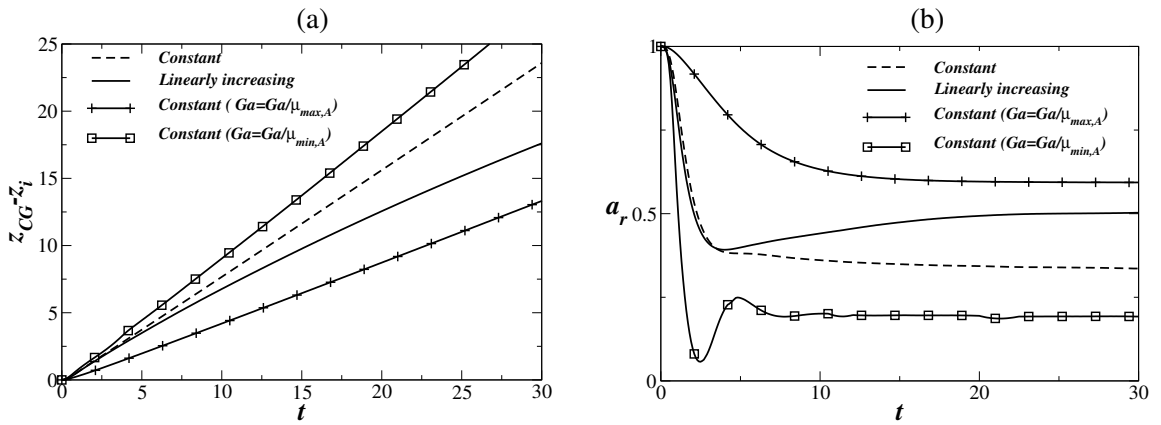


Figure 3.17: Variation of center of gravity and aspect ratio of the bubble with time. The rest of the parameter values are the same as those used to generate Fig. 3.15.

CHAPTER 4

Conclusions

Here, we have examined the axisymmetric dynamics of bubble rise in an unconfined viscosity stratified medium. An open-source finite-volume flow solver, *Gerris* based on volume-of-fluid methodology is used to investigate the flow, which involves the numerical solution of the equations of mass and momentum conservation, and an equation of the volume fraction of the surrounding fluid. In spite of the large number of studies carried out on bubbles and drops, very few studies have examined the influence of viscosity stratification (to the best of our knowledge none of them isolate the effects of viscosity-stratification) on the bubble rise dynamics. We have presented a library of bubble shapes in the Galilei and the Eötvös numbers plane. The present results (terminal shapes of the bubbles) agree well with those obtained by Tsamopoulos *et al.* (2008) for low Ga and low Eo . The shapes of the bubbles are qualitatively different for higher values of Ga and Eo . This difference may be attributed to the steady state calculations conducted in their study. Our results demonstrate a counter-intuitive phenomenon that the bubble undergoes extensive deformation by forming elongated skirt for linearly increasing viscosity medium for certain sets of parameter values. This is due to the migration of less viscous fluid, which is trapped inside the wake region bounded by the skirt of the bubble. This dynamics is very different from that observed in constant viscosity medium. We found that for lower values of Eo and Ga , although the bubble moves slowly in case of the linearly increasing viscosity medium, the shapes look very similar to those observed in constant viscosity medium. In future, it will be interesting to investigate this phenomenon in three-dimensions and by conducting experiments.

Bibliography

- BALASUBRAMANIAM, R. 1998 Thermocapillary and buoyant bubble motion with variable viscosity. *International Journal of Multiphase Flow* **24** (4), 679–683.
- BALASUBRAMANIAM, R. & SUBRAMANIAM, R. S. 1996 Thermocapillary bubble migration thermal boundary layers for large marangoni numbers. *International Journal of Multiphase Flow* **22** (3), 593–612.
- BALASUBRAMANIAM, R. & SUBRAMANIAM, R. S. 2000 The migration of a drop in a uniform temperature gradient at large marangoni numbers. *Physics of Fluids (1994-present)* **12** (4), 733–743.
- BEAL, C. *et al.* 1946 The viscosity of air, water, natural gas, crude oil and its associated gases at oil field temperatures and pressures. *Transactions of the AIME* **165** (01), 94–115.
- BHAGA, D. & WEBER, M. E. 1981 Bubbles in viscous liquids: shapes, wakes and velocities. *J. Fluid Mech.* **105**, 61–85.
- BLANCHARD, D. C. 1962 Comments on the breakup of raindrops. *Journal of the Atmospheric Sciences* **19**, 119–120.
- BONHOMME, R., MAGNAUDET, J., DUVAL, F. & PIAR, B. 2012 Inertial dynamics of air bubbles crossing a horizontal fluid–fluid interface. *J. Fluid Mech.* **707**, 405–443.
- BRACKBILL, J., KOTHE, D. B. & ZEMACH, C. 1992 A continuum method for modeling surface tension. *J. Comput. Phys* **100**, 335–354.
- DAVIES, R. M. & TAYLOR, G. I. 1950 The mechanics of large bubbles rising through extended liquids and through liquids in tubes. *Proc. R. Soc. Lond. A* **200**, 375–390.
- GAL-OR, B., KLINZING, G. E. & TAVLARIDES, L. L. 1969 Bubble and drop phenomena. *Industrial & Engineering Chemistry* **61** (2), 21–34.
- GHANNAM, M. T. & ESMAIL, M. N. 1997 Rheological properties of carboxymethyl cellulose. *Journal of applied polymer science* **64** (2), 289–301.
- GOVINDARAJAN, R. & SAHU, K. C. 2014 Instabilities in viscosity-stratified flows. *Ann. Rev. Fluid Mech.* **46**, 331–353.
- KEMIHA, M., OLMOS, E., FEI, W., PONCIN, S. & LI, H. Z. 1991 Passage of a gas bubble through a liquid–liquid interface. *Ind. Eng. Chem. Res.* **46**, 6099–6104.
- MANGA, M. & STONE, H. A. 1995 Low reynolds number motion of bubbles, drops and rigid spheres through fluid–fluid interfaces. *J. Fluid Mech.* **287**, 279–298.

- MERRITT, R. M., MORTON, D. S. & SUBRAMANIAN, R. S. 1993 Flow structures in bubble migration under the combined action of buoyancy and thermocapillarity. *Journal of Colloid and Interface Science* **155** (1), 200–209.
- POPINET, S. 2003 Gerris: a tree-based adaptive solver for the incompressible euler equations in complex geometries. *Journal of Computational Physics* **190**, 572–600.
- POPINET, S. 2009 An accurate adaptive solver for surface-tension-driven interfacial flows. *J. Comput. Phys* **228**, 5838–5866.
- SUBRAMANIAN, R. S. 1981 Slow migration of a gas bubble in a thermal gradient. *AIChE Journal* **27** (4), 646654.
- SUBRAMANIAN, R. S. 1983 Thermocapillary migration of bubbles and droplets. *Advances in Space Research* **3** (5), 145–153.
- SUBRAMANIAN, R. S., BALASUBRAMANIAM, R. & WOZNIAK, G. 2002 Fluid mechanics of bubbles and drops. In *Physics of Fluids in Microgravity* (ed. R. Monti), pp. 149–177. London: Taylor and Francis.
- SUSSMAN, M. & SMEREKA, P. 1997 Axisymmetric free boundary problems. *Journal of Fluid Mechanics* **341**, 269–294.
- TRIPATHI, M., SAHU, K., KARAPETSAS, G., SEFIANE, K. & MATAR, O. 2015a Non-isothermal bubble rise: non-monotonic dependence of surface tension on temperature. *Journal of Fluid Mechanics* **763**, 82–108.
- TRIPATHI, M. K., SAHU, K. C. & GOVINDARAJAN, R. 2014 Why a falling drop does not in general behave like a rising bubble. *Nature Scientific Reports* **4**, 4771.
- TRIPATHI, M. K., SAHU, K. C., KARAPETSAS, G. & MATAR, O. K. 2015b Bubble rise dynamics in a viscoplastic material **222**, 217–226.
- TSAMOPOULOS, J., DIMAKOPOULOS, Y., CHATZIDAI, N., KARAPETSAS, G. & PAVLIDIS, M. 2008 Steady bubble rise and deformation in newtonian and viscoplastic fluids and conditions for bubble entrapment. *J. Fluid Mech.* **601**, 123–164.
- URBAIN, G., BOTTINGA, Y. & RICHEL, P. 1982 Viscosity of liquid silica, silicates and alumino-silicates. *Geochimica et Cosmochimica Acta* **46** (6), 1061–1072.
- YOUNG, N. O., GOLDSTEIN, J. S. & BLOCK, M. J. 1959 The motion of bubbles in a vertical temperature gradient. *Journal of Fluid Mechanics* **6** (03), 350–356.
- ZHANG, L., SUBRAMANIAN, R. S. & BALASUBRAMANIAM, R. 2001 Motion of a drop in a vertical temperature gradient at small marangoni number the critical role of inertia. *Journal of Fluid Mechanics* **448**, 197–211.